Energy distributions of emitted ion fragments following C(1s) excitations in CO

P. Erman, A. Karawajczyk, U. Köble, E. Rachlew-Källne, and K. Yoshiki Franzén
Department of Physics I, Royal Institute of Technology, S-10044 Stockholm, Sweden
(Received 4 August 1995)

Ion-branching ratios following the relaxation of C $(1s^{-1}\pi^*, nl\lambda, v')$ synchrotron light-excited, vibrationally resolved resonances in CO have been measured using a time-of-flight spectrometer at high extraction voltages. Additional measurements at low extraction voltages (higher kinetic-energy resolution) have enabled an estimate of the kinetic-energy distributions (KED's) of the emitted C^+, O^+, C^{2+}, and O^{2+} ions. Large differences in these distributions are observed at various resonances and, for instance, a doorway-state dependence of the KED has been found for the $3s\sigma$ and $3p\pi$ Rydberg resonances. While the results give some different information concerning the involved relaxation processes, more theoretical calculations are needed to get a more quantitative understanding.

PACS number(s): 33.80.Eh, 33.80.Gj

I. INTRODUCTION

Selective photon excitation of inner-shell electrons in free molecules yields ionization and dissociation via rapid multielectron processes. Observations of such selective bond breaking in molecules give important information about molecular structure and dynamics and have important applications to, for instance, photochemistry and surface physics. Application of high-intensity soft-x-ray radiation from synchrotron undulators in connection with high-resolution ($\geqslant$3000) monochromators has recently made possible studies of the vibrational structure in the decay of core-excited valence and Rydberg states. Studies of this kind have particularly been devoted to the CO molecule where, for instance, the total ion yield has been measured in the vicinity of the C(1s) and O(1s) thresholds [1,2]. However, more information can be extracted if the yields may be studied for each separate ion formed in the core-excited molecule. This has been done very recently at vibrational resolution for the CO molecule using a quadrupole mass spectrometer (QMS) [3] or a time-of-flight (TOF) spectrometer [4].

In the present work we have repeated our QMS measurements [3] using a newly constructed TOF spectrometer with comparatively long drift tube and a grid system which allows operation at low acceleration voltages. In this way the kinetic distributions of the ions can be extracted at higher-energy resolution and the aim of the present work is to deduce these distributions at vibrational resolution for the main resonances excited from the C(1s) shell in CO. We have also remeasured the ion-branching ratios at these resonances at high collection voltages which ensures a high collection efficiency independent of the kinetic energies of the fragments.

II. EXPERIMENTAL PROCEDURE

The present experiments were carried out at the undulator beam line 51 at the MAX laboratory in Lund, Sweden. A commercial SX700 monochromator was used at resolution $\geqslant$6000 and the light intensity was continuously monitored using a calibrated silicon diode detector. The ions were detected using a newly constructed TOF spectrometer where the ions are extracted in two steps in using electric fields F_1 and F_2 followed by a 20-cm-long drift path to a channel plate detector with $\phi = 2$ cm. The ion detector was coupled in coincidence with an electron detector close to the excitation region which triggers the TOF measurements. To avoid any sensitivity to low-energy electrons in the TOF signal, the electrons are accelerated with a few tens of volts per mm before being detected. The axis of the TOF is parallel to the $\vec{E}$ vector of the exciting synchrotron light.

Figure 1 shows portions of the total-ion-yield spectrum of CO measured using the present experimental setup including some of the resonances studied in the present work. The resolution is comparable to the earlier total-yield spectra [1,2] and the vibrational structure is well resolved. The strong enhancement of the π^* ($v = 4$) resonance observed in our QMS studies [3] is well reproduced also in the present TOF spectra and is still waiting for an explanation.

Figure 2 shows two partial TOF spectra recorded at a photon energy of 298.3 eV, and the displayed TOF region includes CO^{2+} and the fragments C^+ and O^+. Figure 2(a) has been recorded with $F_1 = 40$ V/mm and $F_2 = 150$ V/mm,

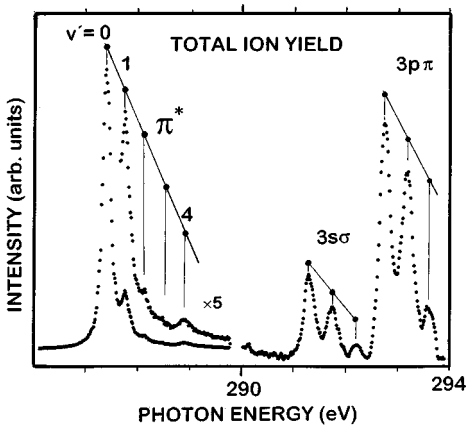

FIG. 1. Total ion yield following C(1s) photon excitation of CO in the range 286–294 eV including the π^*, $3s\sigma$, and $3p\pi$ resonances and their vibrational structure.

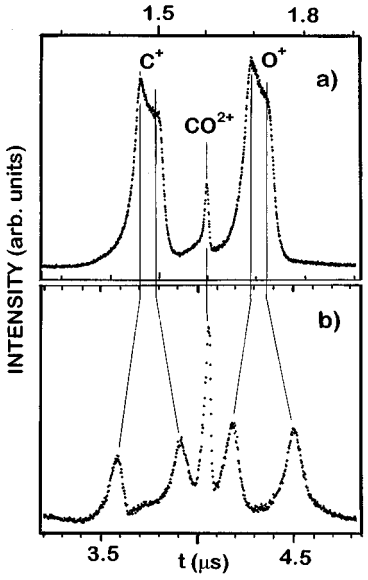

FIG. 2. Partial TOF spectra following photon excitation of CO at 298.3 eV recorded at different extraction fields. (a) $F_1=40$ V/mm, $F_2=150$ V/mm, (b) $F_1=6$ V/mm, $F_2=23.5$ V/mm. The kinetic-energy distributions of the C^+ and O^+ fragments are 6.5 times better resolved at the lower extraction fields.

and Fig. 2(b) with 6 and 23.5 V/mm, respectively. The time scales have been adjusted so that the positions of the zero-kinetic-energy ions coincide. The CO^{2+} ions are emitted with thermal energies and the associated line shape (FWHM=Γ) may accordingly be used as an instrumental line profile in the deconvolution of the atomic ion distribution. In Fig. 2 the latter distribution consists of two components for both C^+ and O^+, the left ones consisting of ions emitted towards the TOF ($\Theta \leqslant 90°$ in Fig. 3), the right ones with $\Theta \geqslant 90°$. It follows from Fig. 2 that the energy resolution is about 6.5 times better at the lower extraction field, which is therefore used in the deconvolutions of the energy distributions.

When an atomic ion is emitted with a certain distribution $N(E)$, it is detected by the TOF spectrometer with a certain efficiency, which depends on its kinetic energy E, the asymmetry parameter β, the emission angle Θ, the extraction fields F_i, and the acceptance angle of the TOF. For a given resonance, in polar representation the emission probability

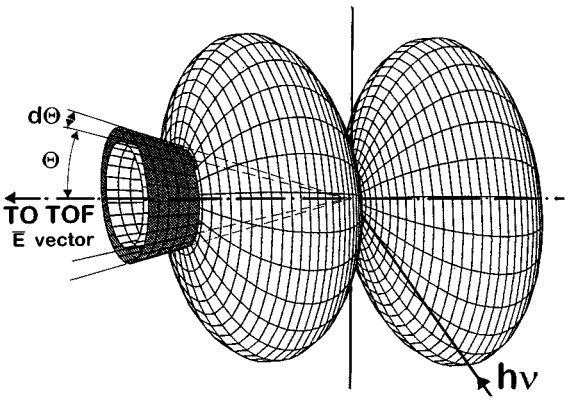

FIG. 3. Deduction of the detection efficiency of the TOF spectrometer as a function of the kinetic energy of the emitted ion and the β parameter of the excited resonance. The figure shows the extreme case when $\beta=+2$ and no ions are emitted perpendicular to the $\bar{E}$ axis ($\Theta=90°$). The scale along the $\bar{E}$ axis is compressed as compared to the remaining axes. In view of the circular symmetry of the TOF and the detector, all the ions M^{q+} of a given energy emitted in the cone within the angular interval Θ and $\Theta+d\Theta$ are detected with equal probability.

varies as $I \propto 1+0.5\beta(3\cos^2\Theta-1)$, which in three dimensions forms a cone for the total emission in the interval Θ to $\Theta+d\Theta$ (Fig. 3). This cone is accepted by the TOF provided that Θ does not exceed a certain value Θ_c, which is calculated from F_1 and F_2 and the dimensions of the TOF and its circular detector for various kinetic energies of a given ion. In this way the detection efficiency $\epsilon(E,\beta,F_i)$ of the TOF is calculated for a certain ion with kinetic energy E and a given β value of the excited resonance. In the deconvolution procedure we then start by assuming a certain distribution $N(E)$, and for equidistant time intervals $\Delta t=\Gamma/2$ the ions are assumed to be detected with the instrumental line profile and the calculated efficiencies ϵ. The sum of all these curves should then constitute the measured TOF distribution. In practice this procedure proceeds in successive iteration steps where $N(E)$ is modified until the best agreement with experiments is obtained.

III. RESULTS AND DISCUSSION

In the present photoionization experiments on CO, the following reactions may occur:

$$\left.\begin{array}{lll} h\nu\ (>287\ \text{eV}) & +\text{CO}\rightarrow & \text{C}(1s^{-1}\pi^*) \\ h\nu\ (>293\ \text{eV}) & +\text{CO}\rightarrow & \text{C}(1s^{-1}nl\lambda) \\ h\nu\ (>296\ \text{eV}) & +\text{CO}\rightarrow & \text{C}(1s^{-1}\sigma^*) \\ & & \text{C}(1s^{-1}5\sigma^{-1}\pi^*nl\lambda) \\ & & \text{C}(1s^{-1}\pi^{-1}\pi^*nl\lambda) \end{array}\right\} \begin{array}{ll} \text{CO}^+, & (1a) \\ \text{C}^+ + \text{O}, & (1b) \\ \text{O} + \text{C}^+, & (1c) \\ \text{CO}^{2+}, & (2a) \\ \text{C}^+ + \text{O}^+, & (2b) \\ \text{C}^{2+} + \text{O}, & (2c) \\ \text{C} + \text{O}^{2+}, & (2d) \\ \text{CO}^{3+}, & (3a) \\ \text{C}^{2+} + \text{O}^+, & (3b) \\ \text{C}^+ + \text{O}^{2+}. & (3c) \end{array}$$

TABLE I. Ion-branching ratios following C(1s) excitation in CO to upper resonances.

Resonance	C^+	O^+	C^{2+}	O^{2+}	CO^+	CO^{2+}
$\pi^* v=0$	0.470(10)	0.314(10)	0.090(3)	0.039(2)	0.074(10)	0.013(4)
$v=1$	0.459	0.342	0.075	0.046	0.056	0.012
$v=2$	0.478	0.321	0.092	0.036	0.056	0.007
$v=3$	0.471	0.331	0.093	0.045	0.053	0.007
$v=4$	0.487	0.318	0.086	0.048	0.051	0.01
$3s\sigma$ $v=0$	0.426	0.450	0.072(6)	0.025(5)	0.025(5)	0.002(1)
1	0.390	0.479	0.079	0.023	0.023	0.005
2	0.360	0.502	0.083	0.036	0.018	0.002
$3p\pi$ $v=0$	0.333	0.461	0.145	0.052	0.005	0.004
1	0.344	0.427	0.154	0.061	0.009	0.005
2	0.357	0.460	0.127	0.038	0.015	0.003
$4p\pi$ $v=0$	0.377	0.439	0.122	0.031	0.023	0.008(3)
Average 298.59 eV -302.91 eV	0.375	0.401	0.160(10)	0.041	0.006	0.017
Ref. [5]						
$\pi^* \bar{v}$	0.546(8)	0.324(8)	0.043(3)	0.014(2)	0.068(5)	0.006(2)
305 eV	0.424(7)	0.419(7)	0.088(3)	0.027(2)	0.030(4)	0.011(2)

The ion-branching ratios at the various resonances were measured using the high-extraction field and they are displayed in Table I. These ratios are corrected for the valence excitation background which was measured at $h\nu \leqslant 285$ eV, i.e., well below the first (π^*) resonance. While being small at the π^* ($v=0$) resonance, this background is substantial at higher resonances, in particular for CO^+ and CO^{2+} ions. Apart from the Rydberg resonances C($1s^{-1}nl\lambda$) converging to the CO^+ ground state, the branching ratios were also measured above the C(1s) ionization limit at 296 eV. A dense line structure appears in this region originating from doubly excited Rydberg resonances superimposed on the well known, broad σ^* resonance (cf. Refs. [1–5]). The branching ratios appeared to remain fairly constant in the 298–305-eV region. Unfortunately, no other measured branching ratios seem to be available for a comparison, except for an early study [5] of the π^* ($v=0$) and ''305'' eV resonance, the results of which are also displayed in Table I.

In the high-resolution measurements by Saito *et al.* [4], TOF spectra of CO^+ and CO^{2+} were measured as well as the pairs $C^+ + O^+$ and $C^{2+} + O^{2+}$ in coincidence runs. However, since the ratios $I(C^+ + O^+)_{\text{pair}} / I(\Sigma C^+ + \Sigma O^+)_{\text{total}}$ are unknown (except possibly for $\pi^*, v=0$), no comparisons can be made between Table I and the spectra displayed in Ref. [4].

The energy distributions of the atomic ion fragments are deduced from the low-field TOF spectra in the manner described in Sec. II. Figure 4 shows the TOF spectra at the resonances π^*, $3s\sigma$, and $3p\pi$ ($v=0$) region of C^+ and O^+. As seen from Fig. 4 (and from Fig. 2) the TOF spectra are very different for the various resonances and, for a given resonance, the C^+ and O^+ distributions are also different.

In deconvoluting the TOF spectra to the ''real'' energy distributions of the ions, we also have to assign β parameters to the various resonances. These are taken from the measurements by Bozek *et al.* [6], which give $\beta(\pi^*) = -0.8$, $\beta(3s\sigma) = 0.4$, $\beta(3p\pi) = -0.4$, and $\beta(\sigma^*) = 0.5$ with a given uncertainty of ± 0.2. The energy distributions $N(E)$ of the atomic ions deduced in this way are shown in Fig. 5. For each resonance the integrated intensities of the fragments have been normalized to the branching ratios given in Table

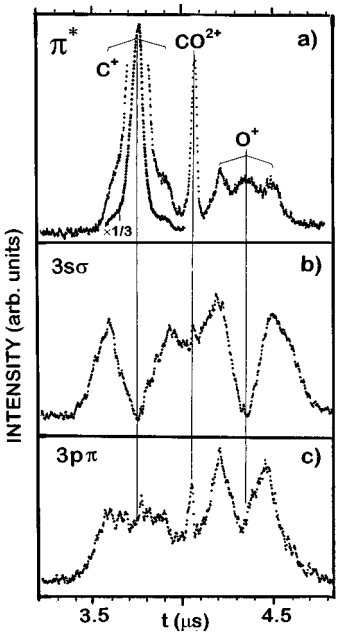

FIG. 4. Partial TOF spectra following C(1s) excitation in CO to the $v'=0$ levels of the π^*, $3s\sigma$, and $3p\pi$ resonances.

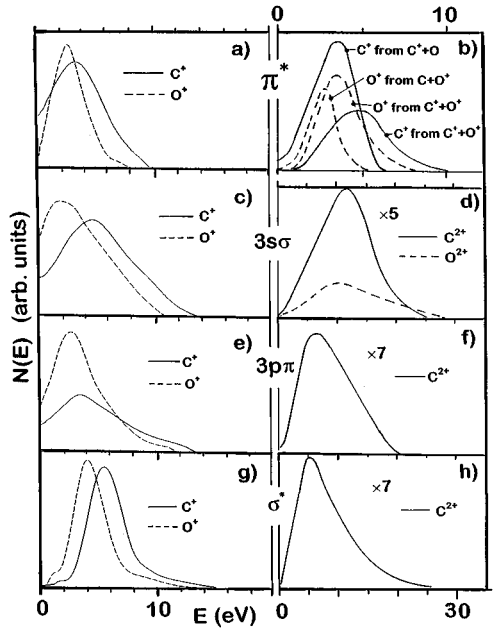

FIG. 5. Energy distributions of C^+, O^+, C^{2+}, and O^{2+} ions following relaxation of the $C(1s^{-1},\pi^*,nl\lambda,\sigma^*)$ resonances in CO as deduced from the low-field extraction TOF spectra (Figs. 2 and 4). The integrated intensities for a given resonance have been normalized to the measured branching ratios and the intensity scales for the doubly charged fragments have been magnified with the displayed factors. The π^*, $3s\sigma$, and $3p\pi$ resonances refer to $v'=0$, but additional measurements for $v'>0$ show very similar distributions for a given resonance. The decomposition of the π^* $v'=0$ resonance into ions formed from dissociations in ion-neutral and ion-ion pairs (b) has been accomplished using ion-ion coincidence data [5].

I. If the β values are varied within the given uncertainties, the distributions do not change significantly, except for $E\geqslant 6$ eV, where, for instance, a reduction of $\beta(3p\pi)$ from -0.4 to -0.6 yields a 10% increase of $N(E)$.

A. π^* resonance

The π^* resonance is the only excitation which gives a considerable fraction of CO^+ ions (Table I), while C^{2+} and O^{2+} are so weak in the low-field runs that no distributions may be deduced. Stable CO^+ ions are produced in participator decay processes to the lowest CO^+ states $X\ ^2\Sigma^+$, $A\ ^2\Pi$, and $B\ ^2\Sigma^+$, while C^{2+} and O^{2+} are formed in the double ionization processes (2c) and (2d). However, all the processes (2a), (2c), and (2d) are far less abundant than decays into $C^+ + O^+$ pairs (2b) (cf. Ref. [5]).

The low-field TOF spectrum of the π^* ($v'=0$) resonance [Fig. 4(a)] shows a very strong central peak for the C^+ ions, which indicates that there are many more low-energetic C^+ ions than O^+ ions [Fig. 5(a)]. All the C^+ distributions shown in Fig. 5 are composed of two main constituents, namely, C^+ formed in dissociations to $C^+ + O$ or $C^+ + O^+$ (ion pairs) [reactions (1b) and (2b), respectively]. In the same way O^+ is formed either from dissociations to $C + O^+$ or $O^+ + O^+$. Ions formed in ion pairs have an excess energy from Coulomb repulsions which might be considerable if the dissociation takes place at a small internuclear distance. For instance, a dissociation into $C^+ + O^+$ pairs in CO at the equilibrium distance ($R_e = 1.15$ Å) gives C^+ and O^+ ions with a Coulomb energy of 7.1 and 5.4 eV, respectively. At $R = 5$ Å, the corresponding energies are 1.7 and 1.2 eV, respectively. In the case of $\pi^* v=0$ the ratios $I(C^+_{\text{pair}})/I(C^+_{\text{total}})$ and $I(O^+_{\text{pair}})/I(O^+_{\text{total}})$ have been established from coincidence measurements [5] to be 0.36 and 0.68, respectively. If we assume that the majority of the energetic ions emerge from dissociations into ion pairs and low-energy ions originate from dissociations into ions plus neutrals, these figures suggest a decomposition of the total distributions of Fig. 5(a) into the partial distributions shown in Fig. 5(b). The contributions from triple ionizations (primarily O^+ from $C^{2+} + O^+$) are small [5] and they are omitted in Fig. 5(b), which should merely be considered as a qualitative description of the atomic ion branchings formed at the $C(1s) \rightarrow \pi^*$ excitation in CO. From Fig. 5(b) we find that the average total energy release at $C^+ + O^+$ pair formation is around 8.7 eV, a value close to what was observed in the coincidence measurements [5], which showed a pronounced maximum at 8.5 eV followed by weaker, secondary peaks at 12.5 and 16.0 eV. The dominating mechanism for producing C^+ and O^+ ions should be spectator decays to two-hole–one-electron ($2h$-$1e$) configurations, in the first place $5\sigma^{-1}1\pi^{-1}2\pi$ and $4\sigma^{-1}5\sigma^{-1}2\pi$. These configurations are dominating in the formation of the $3\ ^2\Sigma^+$ and $D\ ^2\Pi$ states in CO^+, which dissociate into $C^+ + O$ and $C^+ + O$ plus $C + O^+$, respectively. Thus we expect an excess of $[C^+]/([C^+]+[O])$ production relative to $[O^+]/([C]+[O^+])$ production in accordance with the observations. The large excess of low-energy ($\leqslant 2$ eV) C^+ ions can be understood in terms of very recent results from inner-valence-shell excitations of CO with subsequent ion [7] or photoelectron [8] emission. Thus a steep onset of C^+ ion production was observed at the first dissociation limit ($h\nu = 22.34$ eV) [7] and it was attributed to a predissociation caused by a repulsive CO^+ state dissociating to the lowest limit $C^+(^2P^0) + O(^3P)$. In the photoelectron studies [8] it was concluded that this repulsive state probably is $3\ ^2\Pi$, which crosses $D\ ^2\Pi$ at 22.9 eV. Thus most spectator decays to $D\ ^2\Pi$ should give only low-energetic C^+ ions and essentially no O^+ ions. Finally, it should be remembered that an excess of low-energy C^+ ions could also be obtained following a participator decay to a low-lying repulsive CO^+ state.

B. $3s\sigma$ and $3p\pi$ resonances

For all the remaining studied resonances, the O^+ distributions have a lower average energy than the C^+ distributions in the same way as in the case of the π^* resonance. The explanation is probably the same as in the π^* case, i.e., that O^+ ions formed from $(C^+ + O^+)$ pairs get a smaller energy than C^+ ions from pairs at the Coulomb explosions and this effect will displace the total yield curves of C^+ and O^+ accordingly.

The distributions following $3s\sigma(v'=0)$ excitations [Figs. 5(c) and 5(d)] are considerably broader than the remaining distributions. This suggests that the decay of the $3s\sigma$ resonances to a larger extent than the remaining resonances in Fig. 5 leads to CO^{2+} and $(C^{+}+O^{+})$ pair production. To find the reason for this one has to look closer into the different processes leading to double or multiple ionization. In principle two different main processes may occur: one-step double ionization (resonant double Auger) and two-step Auger (two-step autoionization). In the former process two electrons are simultaneously emitted with a continuous energy distribution, while in the two-step process two electrons with well-defined energies are emitted sequentially. It is known from studies of the formation of Kr^{2+} ions from the relaxation of the $Kr^{*}3d^{-1}(^{2}D_{5/2})5p$ resonant state [9] that both processes are present and in this case two-step–one-step branching ratio was found to be 2.3. In the case of the present CO resonances, both processes should also be present. Thus the existence of zero-kinetic-energy electrons from all CO resonances following photon excitation with $h\nu \geqslant 287$ eV [10] suggests that the one-step process is present, while the occurrence of broad lines in the deexcitation electron spectrum of the π^{*} resonance [11] was interpreted [5] in terms of the two-step process. The significant difference between the $3s\sigma$ and $3p\pi$ distributions (Fig. 5) is easier to understand in terms of a participator decay than in a spectator decay since in the latter case the extra $nl\lambda$ electron just contributes with its spin, angular momentum, and screening energy to the holes in the inner shell. However, in a two-step participator process there could possibly be a considerable difference in the decay probabilities of $3s\sigma$ and a $3p\pi$ electron. Moreover, the autoionization of the Rydberg electron competes with dissociation of unstable CO (V^{-2} $3l\lambda$) ions. Since this process is certainly dependent on the position of the core-excited electron, it may partially be ascribed to the observed differences in KED. Thus, we feel that, in spite of the low production of CO^{+} ions at the $C(1s^{-1}nl\lambda)$ resonances (Table I), a substantial amount of two-step participator decays are present, in particular in the case of the $C(1s^{-1}3s\sigma)$ resonances, which lead to double and triple ionization and production of $(C^{+}+O^{+})$, $(C^{2+}+O^{+})$, and $(C^{+}+O^{2+})$ pairs. The excess of the total O^{+} ion production relative to the total C^{+} production in the case of $3p\pi$ indicates that, relative to π^{*} and $3s\sigma$, more dissociations following the decay of $3p\pi$ lead to the limit $C+O^{+}$, i.e., upper states in CO^{+}. Finally, it should be pointed out that the π^{*} and the $nl\lambda$ resonances discussed above also have been studied for $v' \geqslant 0$. However, the deduced energy distributions do not differ significantly from the $v'=0$ distributions in Fig. 5.

C. σ^{*} resonance

Figures 5(a) and 5(b) show the distributions following excitation at 298.3 eV. At this energy, about 2 eV above the $C(1s)$ ionization threshold, the first member ($3s\sigma$) of the doubly excited $C(1s^{-1}5\sigma^{-1}\pi^{*}nl\lambda)$ Rydberg resonances is excited as well as the broad σ^{*} shape resonance with maximum at 306 eV. As already seen from the TOF spectrum (Fig. 2), very few low-energetic C^{+} and O^{+} ions are emitted at this excitation energy and almost no CO^{+} ions (Table I). The TOF spectra looks very similar in the whole excitation range 298–305 eV. In the same way as for the remaining resonances, a quantitative understanding of Figs. 5(g) and 5(h) is possible by considering the Auger spectra and the potential curves of the CO molecule. We observe the first kinetic-energy distribution (KED) component corresponding to the total release energy of ~4.3 eV, which may be ascribed to the dissociation of the P state into $C(^{2}P)+O(^{4}S)$ channel. The low intensity of this component supports the assignment of the Auger peaks as proposed by Liegener [12]. Since the states $^{1}\Pi$ and $^{3}\Sigma^{+}$ have been found to be stable, at least on the microsecond time scale, the expected strongly dissociating configurations are $1\pi^{-2}$ and $4\sigma^{-1}5\sigma^{-1}$, which should yield ions of the total release kinetic energy of 8–10 eV. This is in good agreement with the observed positions of the maximum of the C and O KED curves.

The distributions in Fig. 5 may explain some peculiar features in our earlier measurements [3] using a QMS spectrometer. Thus in the latter measurements an intensity ratio $3p\pi$:$3s\sigma$ of 3.6 was found for O^{+} ions but only 0.8 for C^{+} ions. Also, a large dip was observed in the C^{+} spectrum at around 298 eV but not in the O^{+} spectrum. If we assume that the QMS spectrometer in the experiments [3] only accepts ions with kinetic energies $\leqslant 4$ eV, the distributions in Fig. 5 show that there will always be an excess of detected O^{+} ions as compared to C^{+} ions. However, this excess is considerably larger for $3p\pi$ than for $3s\sigma$ as seen from Figs. 5(c) and 5(e), i.e., relatively more C^{+} ions are lost at $3p\pi$ in accordance with our QMS observations. This difference in C^{+} versus O^{+} detection efficiency is even more pronounced at 298 eV [Fig. 5(g)], where the QMS detects the C^{+} ions with much lower efficiency and contributes to the abovementioned dip in the QMS spectrum.

IV. CONCLUSIONS

The present experiments confirm that energy distributions of ion fragments following inner-shell excitations may be determined from TOF mass spectroscopy and the joint knowledge from runs using low and high-extractions fields. Obvious improvements of the present experiment are the introduction of coincidence measurements and position-sensitive detectors. The measured energy distributions of C^{+}, O^{+}, C^{2+}, and O^{2+} following $C(1s)$ excitation to the CO π^{*} valence state and Rydberg levels $nl\lambda$ show significant differences, which may only be partially understood at the present state of theoretical knowledge.

ACKNOWLEDGMENTS

This research has been supported by grants from the Swedish Natural Science Research Council (NFR) and from the Göran Gustafsson Foundation. We also wish to thank the staff at MAX lab for support and in particular Ergo Nömmiste and Seppo Aksela for the support at the beamline. We have also benefitted from discussions with T. Åberg during his visit to KTH supported by the Nordisk Forskerutdannelseakademi (NORFA).

[1] M. Domke, C. Xue, A. Puschmann, T. Mandel, E. Hudson, D. A. Shirley, and G. Kaindl, Chem. Phys. Lett. **173**, 122 (1990); **174**, 668 (1990).

[2] Y. Ma, C. T. Chen, G. Meigs, K. J. Randall, and F. Sette, Phys. Rev. A **44**, 1848 (1991).

[3] P. Erman, A. Karawajczyk, E. Rachlew-Källne, and C. Strömholm, J. Phys. B **28**, 2069 (1995).

[4] N. Saito, F. Heiser, O. Hemmers, A. Hempelmann, K. Wieliczek, J. Viefhaus, and U. Becker, Phys. Rev. A **51**, R4313 (1995).

[5] A. P. Hitchcock, P. Lablanquie, P. Morin, E. Lizon, A. Lugrin, M. Simon, P. Thiry, and I. Nenner, Phys. Rev. A **37**, 2448 (1988).

[6] J. D. Bozek, N. Saito, and I. H. Suzuki, J. Chem. Phys. **100**, 393 (1994).

[7] P. Erman, E. Rachlew-Källne, and S. Sorensen, Z. Phys. D **30**, 315 (1994).

[8] P. Baltzer, M. Lundqvist, B. Wannberg, L. Karlsson, M. Larsson, M. A. Hayes, J. B. West, M. R. F. Siggel, A. C. Parr, and J. L. Dehmer, J. Phys. B **27**, 4915 (1994).

[9] P. Lablanquie and P. Morin, J. Phys. B **24**, 4349 (1991).

[10] L. J. Medhurst, P. A. Heimann, M. R. F. Siggel, D. A. Shirley, C. T. Chen, Y. Ma, S. Modesti, and F. Sette, Chem. Phys. Lett. **193**, 493 (1992).

[11] W. Eberhardt, E. W. Plummer, C. T. Chen, and W. K. Ford, Austr. J. Phys. **39**, 853 (1986).

[12] C. M. Liegener, Chem. Phys. Lett. **106**, 201 (1984).